Title
Superposition of Fragment Excitations for Excited States of Large Clusters with Application to Helium Clusters.

Journal
Journal of chemical theory and computation, 11(12)

ISSN
1549-9618

Authors
Closser, Kristina D
Ge, Qinghui
Mao, Yuezhi
et al.

Publication Date
2015-12-01

DOI
10.1021/acs.jctc.5b00703

Peer reviewed

An excited state method using absolutely localized molecular orbitals with application to spectra of large helium clusters

Journal:	*Journal of Chemical Theory and Computation*
Manuscript ID	ct-2015-00703c.R1
Manuscript Type:	Article
Date Submitted by the Author:	02-Oct-2015
Complete List of Authors:	Closser, Kristina; University of California, Berkeley, Chemistry; Lawrence Berkeley National Laboratory, Ge, Qinghui; University of California, Berkeley, Chemistry; Lawrence Berkeley National Laboratory, Mao, Yuezhi; University of California, Berkeley, Chemistry Shao, Yihan; Q-Chem Inc, Head-Gordon, Martin; University of California, Berkeley, Chemistry; Lawrence Berkeley National Laboratory,

An excited state method using absolutely localized molecular orbitals with application to spectra of large helium clusters

Kristina D. Closser,[†,‡,§] Qinghui Ge,[†,‡] Yuezhi Mao,[†] Yihan Shao,[¶] and Martin Head-Gordon[*,†,‡]

Kenneth S. Pitzer Center for Theoretical Chemistry, Department of Chemistry, University of California, Berkeley, CA 94720,

Chemical Sciences Division, Lawrence Berkeley National Laboratory, Berkeley, CA 94720, and Q-Chem Inc, 6601 Owens Drive, Suite 105, Pleasanton, California 94588, USA

E-mail: mhg@cchem.berkeley.edu

Abstract

We develop a local excited state method, based on the configuration interaction singles (CIS) wavefunction, for large atomic and molecular clusters. This method exploits the properties of absolutely localized molecular orbitals (ALMOs), which strictly limits the total number of excitations, and results in formal scaling with the third power of

[*]To whom correspondence should be addressed
[†]University of California, Berkeley
[‡]Lawrence Berkeley National Laboratory
[¶]Q-Chem Inc
[§]Current address: Materials Sciences Division, Lawrence Berkeley National Laboratory

the system size for the computation of the full spectrum of ALMO-CIS excited states. The derivation of the equations and design of the algorithm are discussed in detail, with particular emphasis on the computational scaling. Clusters containing nearly 500 atoms were used in evaluating the scaling, which agrees with the theoretical predictions, and the accuracy of the method is evaluated with respect to standard CIS. A pioneering application to the size dependence of the helium cluster spectrum is also presented for clusters ranging from 25 to 231 atoms, the largest of which results in computation of 2310 excited states per sampled cluster geometry.

1 Introduction

Predicting the electronically excited states of large systems with reasonable accuracy is an ongoing challenge for quantum chemistry. The competition between accuracy and efficiency places significant limitations on the methods that are practically useful.[1,2] By far the most widely used method for computing excited states of medium-sized and larger molecules is time-dependent Kohn-Sham density functional theory (TD-DFT).[3,4] This method involves computational effort per state which is similar to the effort required to treat the ground state by DFT. Formally, a quadratic number of variables, akin to single excitations, are involved, and the computational cost typically grows between the square and the cube of system size per state. Thus calculations of roughly 5-40 states are manageable if the corresponding ground state calculation is feasible. On the other hand, obtaining *all* excited states requires computational effort that rises asymptotically with the sixth power of molecular size, which rapidly becomes unfeasible even when the ground state calculation is tractable. The accuracy of TD-DFT calculations is also limited by the well-known difficulty in systematically improving present-day density functionals. Incorrect asymptotic potentials cause errors in the position of Rydberg excited states, while self-interaction errors yield dramatic failures for charge transfer excited states, although to some extent this can be remedied by using

modern range-separated density functionals.[2,5–8]

In contrast, wave-function based approaches to excited states are appealing in that they can be straight-forwardly improved through incorporation of additional degrees of freedom, typically in the form of higher substitutions through a configuration interaction (CI) wave function. Due to the Brillouin Theorem, the variationally optimized mean field Hartree-Fock wavefunction has matrix elements which are strictly zero, with all singly substituted configurations. Thus, the simplest CI wavefunction for excited states is CI in the space of single substitutions (CIS):[3,9]

$$|\Psi\rangle = \sum_s c_s |\Phi_s\rangle \tag{1}$$

CIS has half the number of degrees of freedom of TD-DFT (identical within the Tamm-Dancoff approximation[10]), thus its computational cost is roughly comparable. Relative to TD-DFT with commonly available functionals, CIS has the advantage of a correct asymptotic potential and zero self-interaction error. However, it completly neglects dynamic electron correlation, which leads to errors in valence excitation energies that are on the order of 1 eV (the correlation energy for a pair of electrons).

More sophisticated wave-function methods introduce additional complexity to account for electron correlation effects through double and higher substitutions. The simplest methods are perturbative cousins to CIS such as the non-degenerate CIS(D) correction,[11] and its quasi-degenerate variants.[12] The latter relate closely to the second order coupled cluster approximation (CC2),[13] which is itself an approximation to full equation of motion coupled-cluster (EOM-CC) theory (e.g. EOM-CCSD, EOM-CCSD(T)).[14,15] The cost of the additional electron correlation can be as low as fourth order in system size for scaled opposite spin methods,[16,17] while it is fifth order for the full perturbative methods,[11] and sixth order with complete iterative treatment of the doubles. Iterative triples methods scale with the eighth power of system size. Such steep increases in computational cost with system

size place increasingly severe restrictions on the systems that can be successfully treated. Even so, the above methods (including TD-DFT) fail for problems where the ground state is not well approximated by a good single configuration, and these must be addressed by active space methods such as the complete active space self-consistent field method (CAS-SCF) and the corresponding second order perturbative corrections,[18,19] or with spin-flipping methods.[20–22]

Great effort has gone into reducing the computational requirements of electronic structure theory calculations for the ground state from quadratic storage and cubic computation towards linear scaling. As argued by Kohn,[23] the 1-particle density matrix that controls the ground state energy is intrinsically "short-sighted" and therefore in the large system limit, only a linear number of variables are significant. While linear scaling methods for forming the effective Hamiltonian have been widely used since the early 1990's,[24–26] linear scaling replacements for diagonalization, though extensively developed,[27] are not widely applied, primarily because extremely large systems are needed to realize adequate sparsity in real space,[28] and the situation is even more challenging in spectral representations.

Linear scaling methods, while less throughly developed than for ground states, have also been proposed for excited states.[29] Specifically, there have been formulations of CIS and TD-DFT which are appropriate for linear scaling,[30,31] and some proof-of-concept implementations and calculations have been reported.[32–35] However, these methods are not widely used for production calculations at the moment, in part because excited states appear to exhibit substantially greater delocalization then ground states.

Therefore if one is interested in systems significantly larger than 100 atoms, but not large enough that rigorous linear scaling is possible, it is necessary to apply additional approximations.[36] Exploiting the intrinsic locality in certain types of chromophores has led to the development of incremental, multi-layer and fragmentation based approaches.[36–41] Biological systems often fall into this category and reports of heroic calculations with over

20,000 atoms have been reported.[42] However, the excited states for these systems were only computed on fragments containing no more than 103 atoms.

Grimme recently published a simplified method based on the Tamm-Dancoff approximation to TD-DFT (sTDA), where he reported results for a 483 atom/6879 basis function system.[43,44] The two-pronged approach used a Löwdin-monople basis for the two electron integrals and a bold truncation of the single excitations to make this feasible. This integral approximation leads to a preferential description of delocalized states and four global parameters were introduced to reduce some of the systematic error.

Even more recently, Liu and Herbert reported a TD-DFT(MI) method applicable to computing the excited states of large clusters.[45] Conceptually nearly identical to the ALMO-CIS method presented here, their work also focuses on computing excited states of clearly defined chromophores, which couple weakly to surrounding solvent molecules. While in principle their method is extensible to multiple chromophores the algorithm is optimized for computing a relatively small number of the excited states. Helmich and Hättig proposed a method based on truncation of the pair natural orbital (PNO) space.[46,47] Although intriguing their current implementation is still $\mathcal{O}(N^4)$ and not practical for large systems when many states are requested.

Nearly all current implementations of CIS and TD-DFT are optimized for computing a handful of the low-lying excited states, and both the linear scaling and fragment-based methods discussed above for treating larger systems continue in this approach. However, when dealing with large homogeneous systems, such as atomic and molecular clusters, dense manifolds of states with similar energies must be considered, and thus many states (a full description of at least the bands of interest) are required to connect directly to experimental results. In relation to more typical situations where only a few excited states are required, this increases the scaling of the computational cost by at least one power of system size. Such non-covalently bound clusters have generated significant interest as they span the

range between the gas phase and bulk limits, and are useful for investigating fundamental differences between bulk and surface properties.[48–50]

The excitation energies of rare gas clusters, have attracted great interest due to their unique properties. Helium clusters in particular are extremely cold, superfluidic,[51] and when used as a spectroscopic medium provide a unique environment that allows rotational resolution of dopant solutes.[52–55] For the electronic spectrum of undoped clusters, the sharp atomic lines (e.g. $2p$ and $3p$) of the helium atom give way to broad blue-shifted peaks in large clusters,[56] which correspond to bands of excited states. The photoionization dynamics of these clusters have also been the subject of considerable recent interest.[57]

Here we report the development of a local excited state method that can adequately describe large numbers of electronic excited states (as needed to describe the bands) of large atomic and molecular clusters at greatly reduced computational cost. In a 1000 atom cluster, the n=2 band would require a minimum of 4000 states to describe correctly. This situation where the number of states increases with cluster size is one that conventional molecular excited state codes are quite unsuited to handle, and it introduces an enormous additional pre-factor to the computational cost. At the same time, because each atom in such a cluster is identical, there is no obvious locality to the excited states: in general they may be fully delocalized throughout the cluster. Both of these factors make the development of a viable computational method potentially very challenging.

There is one critically important physical advantage that we can exploit to make the problem tractable. We have previously reported on the electronically excited states of small helium clusters using standard configuration interaction singles (CIS).[58,59] In the $n = 2$ manifold, we determined that the excited states could be interpreted in terms of superpositions of atomic-like excitations.[58] This is perhaps not too surprising because of the very high ionization energy of He atoms, and the fact that the electron affinity is negative. This characteristic of the excited states suggests that the states associated with the $2p$ and $3p$

bands may be adequately described as superpositions of atomically localized excitations. Such a model has storage requirements that grow linearly per state, and only quadratically for all states. The computational cost then grows no worse than the cube of the number of atoms to obtain the full spectrum of excitations.

The theory presented here is optimized for clusters consisting of identical fragments, which may be atomic or molecular clusters (e.g. nitrogen clusters, or even water clusters, may be reasonably well described). Previously, the ground state of a strongly localized molecular cluster was shown to be quite accurately treated at greatly reduced computational cost through the use of absolutely localized molecular orbitals (ALMOs).[60] The ALMO approximation is that the MO coefficient matrix is defined to be block diagonal in the molecules comprising the cluster.[61–64] Thus each MO on a given molecule is a superposition of only AO's centred on the same molecule. In addition to accelerating SCF calculations for large systems,[60] ALMO's have been used for calculating the individual contributions to intermolecular interactions.[65–68] A direct result of the ALMO approximation is that ALMO's are non-orthogonal between fragments.

ALMOs are an ideal basis within which to define a variant of CIS in which states are defined as superpositions of intra-fragment excitations. By allowing excitations only within the orbital space of a given fragment, charge-transfer between fragments is prohibited and the number of singly excited states used for the calculation grows linearly with cluster size (for a homogeneous cluster). As a result, far larger clusters can be examined than would otherwise be possible. In this paper we formulate the theory for this local ALMO-CIS method, and discuss an efficient cubic scaling implementation that yields all the ALMO-CIS states via direct diagonalization after constructing the corresponding Hamiltonian. We present benchmarks showing the extent to which ALMO-CIS calculations are faithful to full CIS calculations for helium clusters, with satisfactory results. Timings for the algorithm are presented for helium clusters containing nearly 500 atoms. We also include initial results

using the ALMO-CIS method to explore the size dependence of the excitation spectrum of helium clusters with a more thorough report on these systems to appear in an subsequent publication.

2 Theory

2.1 Notation

Tensors provide a useful notion for treating non-orthogonal functions, such as the ALMO's. Thus, standard tensor notation is used,[69,70] where subscripts indicate functions in the covariant (given) basis, and superscripts indicate functions in the (biorthogonal) contravariant space. The Einstein summation convention is also employed, where an index that occurs once covariant and once contravariant, implies a sum.

Occupied molecular orbitals (MO's) are denoted as i, j, k, virtual orbitals as a, b, c and general orbitals as p, q, r. ALMOs will be represented using $|\psi\rangle$, and later it will be necessary to form a set of projected ALMOs which will be distinguished using $|\phi\rangle$ and Greek subscripts (note that for occupied orbitals, $|\phi_\iota\rangle = |\psi_i\rangle$, but for the virtuals $|\phi_a\rangle \neq |\psi_a\rangle$). Atomic orbital (AO) functions are given by χ_μ, auxiliary basis functions (used in resolution of the identity fitting) by χ_Q, and fragments are indicated I, J or F_I, F_J.

Fragment-localized quantities will be made explicit through the use of connecting lines above or below: for instance two MO's p and q are constrained to a single fragment, F_I, if their indexes are connected as $\overbracket{pq}$ or $\underbracket{pq}$. Throughout the discussion of the algorithms, when discussing the scaling, capital letters will denote quantities that scale with the size of the system and lower case letters indicate the value only depends upon the identity of a given fragment. In particular, in our analysis of homogeneous atomic or molecular clusters we shall consider them to contain M identical fragments, and thus the computational effort can be evaluated as a power of M.

2.2 Ground State Wavefunction with Absolutely Localized Molecular Orbitals

The ground-state Hartree-Fock wavefunction is a Slater determinant of one electron functions.

$$|\Psi_0\rangle = |\psi_1 \dots \psi_i \psi_j \dots \psi_n\rangle. \tag{2}$$

For standard electronic structure calculations the ψ_i are canonical MO's, which diagonalize the Fock operator, and are typically highly delocalized. The MO's are expanded in terms of atom-centered basis functions (AO's) as

$$|\psi_p\rangle = \sum_\mu |\chi_\mu\rangle \, c^\mu_{.p}, \tag{3}$$

where the AO's, χ_μ, are assumed to be contracted Gaussians.

The atom-centered AO's used in electronic structure theory calculations are naturally partitioned according to the fragment on which they reside. Absolutely localized molecular orbitals (ALMOs) arise by applying the constraint that the MO coefficient matrix should be fragment blocked, such that the ALMO's which describe an atom or molecule in a cluster contain only contributions from the AO's of that specific fragment.[60] When using ALMOs, each molecular orbital is tagged to a fragment F_J and expanded only in the subset of basis set functions with centers on that fragment.

$$|\psi_p\rangle = \sum_{\mu \in F_J} |\chi_\mu\rangle \, c^\mu_{.p}, \quad p \in F_J. \tag{4}$$

The resulting occupied ALMOs are nonorthogonal between fragments, although the occupied ALMO's on a single fragment can be chosen to be orthogonal. The block-diagonal structure of the ALMO transformation leads to very high computational efficiency. It is highly desirable to maintain this local structure for excited state evaluation, as will be discussed further in

Section 3.3.

In tensor notation, the overlap of non-orthogonal orbitals, such as the ALMO's, is defined by the covariant overlap metric

$$\langle \psi_p \,|\, \psi_q \rangle = \sigma_{pq} = S_{pq} \tag{5}$$

and likewise the contravariant metric is

$$\langle \psi^p \,|\, \psi^q \rangle = \sigma^{pq} = \sigma^{-1}_{pq} = S^{-1}_{pq}. \tag{6}$$

The biorthogonality of the covariant and contravariant subspaces implies

$$\langle \psi^p \,|\, \psi_q \rangle = \delta^p_{\cdot q}. \tag{7}$$

The nonorthogonality of ALMO's between fragments has the interesting implication that the so-called "virtual" ALMO's, $|\psi_a\rangle$, are not strictly virtual, because they overlap occupied ALMO's on other fragments: $\langle \psi_k \,|\, \psi_a \rangle \neq 0$. To obtain well-defined virtual functions, it is necessary to remove contamination in $|\psi_a\rangle$ from the occupied subspace. Projecting the occupied ALMOs $|\psi_k\rangle$ from the virtual ALMOs $|\psi_a\rangle$ yields new (projected) virtuals $|\phi_a\rangle$. The $|\phi_a\rangle$ are orthogonal to all occupied ALMO's by construction, but remain nonorthogonal amongst themselves.

$$\begin{aligned} |\phi_a\rangle =& \mathcal{N}_a \left(|\psi_a\rangle - \hat{P}_{occ} \,|\psi_a\rangle \right) \quad = \mathcal{N}_a \left(|\psi_a\rangle - |\psi_k\rangle \, \sigma^{kl} \, \langle \psi_l \,|\, \psi_a \rangle \right) \\ =& \mathcal{N}_a \left(|\psi_a\rangle - |\psi_k\rangle \, \sigma^{kl} \sigma_{la} \right) = \mathcal{N}_a \left(|\psi_a\rangle - |\psi_k\rangle \, d^k_{\cdot a} \right) \end{aligned} \tag{8}$$

Here $\mathcal{N}_a$ is a normalization factor to ensure $\langle \phi_a \,|\, \phi_a \rangle = 1$, and $d^k_{\cdot a} = \sigma^{kl}\sigma_{la}$.

2.3 Nonorthogonal CIS and the ALMO-CIS model

Singly substituted configurations are formed by promoting an electron from an occupied Hartree-Fock orbital to a virtual orbital that is orthogonal to the occupied one. Note these are the projected orbitals so that they are properly orthogonal to the occupied space.

$$\left|\Psi^{i}_{\cdot a}\right\rangle = |\psi_1 \ldots \phi_a \psi_j \ldots \psi_n\rangle \tag{9}$$

The CIS excited states are superpositions of all single substitutions, with amplitudes $t^{a}_{\cdot i}$:

$$|\Psi_{CIS}\rangle = a^{\dagger}_{a} a^{i} \,|\Psi_0\rangle\, t^{a}_{\cdot i} = \left|\Psi^{i}_{\cdot a}\right\rangle t^{a}_{\cdot i} \tag{10}$$

Substituting this wavefunction into the time-independent Schrödinger equation and projecting with each of the excited determinants according to the linear variational principle yields equations for the CIS excitation energies.

$$\left\langle \Psi^{b}_{\cdot j}\right| \hat{H} \left|\Psi^{i}_{\cdot a}\right\rangle t^{a}_{\cdot i} = \omega_{CIS} \left\langle \Psi^{b}_{\cdot j} \right| \left.\Psi^{i}_{\cdot a}\right\rangle t^{a}_{\cdot i} \tag{11}$$

where $\omega_{CIS} = E_{CIS} - E_0$.

The choice of the natural representation[69] makes evaluation of the matrix elements isomorphic to the conventional orthonormal case, because biorthogonality of covariant and contravariant functions permits similar simplifications. Recalling Eq. (7), we see that:

$$\left\langle \Psi^{b}_{\cdot j} \mid \Psi^{i}_{\cdot a} \right\rangle = \delta^{i}_{\cdot j} \delta^{b}_{\cdot a} \tag{12}$$

Carefully evaluating the matrix elements leads to the following eigenvalue equation in the natural representation (this is a generalized version of the conventional result, where biorthog-

onality replaces orthogonality):

$$A^{ib}_{\cdot\cdot ja} t^{a}_{\cdot i} = \omega_{CIS} \delta^{b}_{\cdot a} \delta^{i}_{\cdot j} t^{a}_{\cdot i} \tag{13}$$

The matrix elements of the singles-singles block of the Hamiltonian are given in the biorthogonal representation as:

$$A^{ib}_{\cdot\cdot ja} = f^{b}_{\cdot a} \delta^{i}_{\cdot j} - f^{i}_{\cdot j} \delta^{b}_{\cdot a} + \left\langle \psi^{i} \phi^{b} \,||\, \phi_{a} \psi_{j} \right\rangle \tag{14}$$

These equations can be transformed to the covariant integral representation (where the unknown amplitudes are fully contravariant, whilst the known matrix elements are fully covariant) using metric matrices to obtain

$$A_{ibja} t^{ai} = \omega_{CIS} S_{ab} S_{ij} t^{ai} \tag{15}$$

$$A_{ibja} = f_{ba} S_{ij} - f_{ij} S_{ba} + \left\langle \psi_{i} \phi_{b} \,||\, \phi_{a} \psi_{j} \right\rangle \tag{16}$$

Introducing the overlap matrix here and transforming to the natural representation preserves the Hermiticity of the Hamiltonian and the variational nature of the wavefunction.

For closed shell singlet wavefunctions, the spin-restricted form, with all dimensions collapsed to those of spatial orbitals rather than spin-orbitals, is:

$$A_{ibja} = f_{ba} S_{ij} - f_{ij} S_{ba} + 2 \left(\psi_{i} \phi_{a} \,|\, \phi_{b} \psi_{j} \right) - \left(\psi_{i} \psi_{j} \,|\, \phi_{b} \phi_{a} \right) \tag{17}$$

The spatial orbital two-electron integrals are written in the "chemist's notation" where the first two indexes involve the coordinates of electron 1 and the last two indexes are those of electron 2.

The non-orthogonal CIS equations, as written, convey computational advantage only when the one and two-electron matrix elements become sufficiently sparse that the dimension

of the problem can be greatly reduced. As argued in the introduction, this is very difficult to exploit computationally except for truly enormous systems. For clusters on the order of 1000 atoms, as may be treated with this theory, there is very little effective sparsity because of the spatially extended basis sets that are needed to treat Rydberg excited states (equivalent to at least doubly augmented basis sets, in terms of the Dunning hierarchy or the (2+) sets in terms of diffuse functions for Pople basis sets).

Instead, we build a physically-based model, akin to local correlation models, which restricts the single substitutions to only occur within fragments. By doing so, we prohibit charge transfer between fragments. In the limit of non-interacting fragments, such a model is exact. As discussed in the introduction, it is also likely to be quite accurate for weakly interacting clusters if their constituent atoms or molecules have high ionization potentials and low (or negative) electron affinities.

We shall refer to this model where the excited states are approximated as superpositions of intra-fragment single substitutions as ALMO-CIS. Considering homogeneous atomic or molecular clusters containing M fragments, it is evident that the ALMO-CIS model retains only $\mathcal{O}(M)$ of the original $\mathcal{O}(M^2)$ CIS amplitudes. Since the model has included locality at the design level, it will also be relatively easy to exploit this great reduction in the computational complexity. The ALMO-CIS equations follow from the non-orthogonal CIS equations in the covariant integral representation by deleting all rows and columns corresponding to single substitutions that transfer charge between fragments:

$$\mathscr{A}_{\underline{ia},\underline{jb}}\, t^{\overline{ai}} = \omega_{CIS}\, \mathscr{S}_{\underline{ia},\underline{jb}}\, t^{\overline{ai}} \tag{18}$$

with

$$\mathscr{A}_{\underline{ia},\underline{jb}} = A_{\underline{\underline{ibja}}} \text{ and } \mathscr{S}_{\underline{ia},\underline{jb}} = S_{\underline{ij}} S_{\underline{\underline{ab}}}. \tag{19}$$

2.4 ALMO-CIS Oscillator Strengths

The oscillator strength for a electronically excited state κ reflects the probability of a transition from the ground state into that state and is generally defined (in atomic units):

$$f_\kappa = \frac{2}{3}(E_\kappa - E_0)\left|\langle \Psi_0 \left|\hat{\mu}\right| \Psi_\kappa \rangle\right|^2 . \tag{20}$$

The energy difference comes directly from the calculation of the ALMO-CIS eigenvalues, and the dipole expectation value is given from the projected ALMOs as

$$\langle \Psi_0 \left|\hat{\mu}\right| \Psi_\kappa \rangle = \sum_{F_J} \sum_{i,a\in\{\Psi_J\}} t_\kappa^{\overrightarrow{ai}} \langle \psi_i \left|\hat{\mu}\right| \phi_a \rangle . \tag{21}$$

The dipole matrix elements can then readily be determined from the available AO basis matrix elements.

$$\langle \psi_i \left|\hat{\mu}\right| \phi_a \rangle = (\psi_i \left|\chi^\mu\right\rangle \langle \chi_\mu \left|\hat{\mu}\right| \chi_\nu \rangle \left\langle \chi^\nu \right| \phi_a) = c_{\cdot i}^{\mu\dagger} \mu_{\mu\nu} c_{\cdot a}^{\nu}. \tag{22}$$

3 Efficient Implementation and Scaling

An efficient implementation of the ALMO-CIS method has been completed within the Q-Chem electronic structure program.[71,72] The following subsections describe the key design aspects of the algorithm we have developed and implemented.

3.1 Direct vs Iterative Diagonalization

The first key design decision is how the truncated Hamiltonian should be diagonalized: directly by dense linear algebra, or iteratively on the basis of matrix-vector multiplies.[73] While

iterative diagonalization is greatly preferred if only a few eigenvalues are desired, direct diagonalization is more efficient if a significant fraction of the eigenvalues are sought. Our first target application of ALMO-CIS is to compute the excited states of large homogeneous clusters. These typically have many excited states within a narrow energy window, corresponding to bands that broaden the discrete excitations of the spectrum of a single fragment, and thus, a large percentage of the CIS eigenvalues are desired.

Therefore we choose direct diagonalization as the basis of this implementation. We note that this is not a serious limitation on the size of system that can be treated via ALMO-CIS, as the ALMO-CIS vectors are $\mathcal{O}(M)$ and thus construction of the ALMO-CIS Hamiltonian requires $\mathcal{O}(M^2)$ storage, and direct diagonalization is $\mathcal{O}(M^3)$ for the full spectrum. By contrast, conventional CIS involves eigenvectors of length $\mathcal{O}(M^2)$ and therefore requires $\mathcal{O}(M^4)$ storage and $\mathcal{O}(M^6)$ computational effort for direct diagonalization. The ALMO-CIS calculation involves storage and computation that is proportional to only the square root of that for conventional CIS. Or for equivalent computational resources, ALMO-CIS will be able to treat a system of $\mathcal{O}(M^2)$ size if conventional CIS can treat a system of size $\mathcal{O}(M)$.

3.2 Strategy for Two-Electron Integral Evaluation

Generally the most computationally demanding step in standard CIS is associated with formation and transformation of the two-electron repulsion integrals (ERI's). There are two basic issues that dictate our strategy. First, is the extent to which basis function overlaps become sparse in a large cluster. Second, is the question of how effective the resolution of the identity (or density fitting) approach is likely to be. We shall discuss these issues in turn, and then outline our chosen approach.

With regard to the first issue, AO-ERI calculations naïvely scale as $\mathcal{O}(M^4)$. In large molecules with compact basis sets, this can be reduced to quadratic cost by applying appropriate screening techniques, such as the Schwarz integrals, which yield a strict upper bound

to the size of the integrals.[74,75]

$$|(\mu\nu \mid \lambda\sigma)| \leq (\mu\nu \mid \mu\nu)^{1/2} (\lambda\sigma \mid \lambda\sigma)^{1/2} \tag{23}$$

The number of significant basis function pairs, with a threshold of $1 \times 10^{-12} E_h$ are shown in fig. 1 as a function of cluster size for regularly spaced helium clusters using the cc-pVTZ basis, aug-cc-pVTZ, and a customized $[5s2p]$ basis (consisting of the 3 s functions of 6-311G and two sets of diffuse s and diffuse p exponents, subsequently denoted 6-311(2+)G) that is suitable for describing the n=2 Rydberg manifold.[58] It is evident that effective linear scaling is not obtained with the diffuse basis set until clusters of well over 1000 atoms as the slope is still larger than 1 even at He_{1159}. By contrast the compact cc-pVTZ basis reaches linear scaling in its number of numerically significant basis function pairs much sooner, around 60 atoms. Therefore excited state calculations which depend on diffuse basis functions face growth in the number of significant AO-ERI's that remains close to $\mathcal{O}(M^4)$ into regimes as large as 1000 atoms. As a result, evaluation of the MO-ERI's by naïve transformation of AO-ERI's would be at least this demanding, and therefore will not be very computationally efficient.

The ALMO-CIS model, however, offers crucial additional computational advantages. The ALMO occupied orbitals and the unprojected virtual orbitals are both fragment blocked, and as a result, *if we ignore the projection terms* the ALMO-CIS model rigorously requires only $\mathcal{O}(M^2)$ AO-ERI's. Let us begin by expanding the Coulomb-like term, $(\psi_i\underline{\phi_a} \mid \psi_j\underline{\phi_b})$, of Eq. (17), in terms of unprojected ALMO contributions and projection corrections:

$$\begin{aligned}(\psi_i\underline{\phi_a} \mid \psi_j\underline{\phi_b}) =& \mathcal{N}_a\mathcal{N}_b \Big\{ (\psi_i\underline{\psi_a} \mid \psi_j\underline{\psi_b}) \\ & -2 \left(\psi_i\underline{\psi_a} \,|\overbrace{\psi_j\psi_k}\right) \left(\psi^k \mid \psi_b\right) + \left(\psi_i\underline{\psi_k} \mid \overbrace{\psi_j\psi_l}\right) \left(\psi^k \,|\underline{\psi_a}\right) \left(\psi^l \,|\overbrace{\psi_b}\right) \Big\} \\ J =& N^2(J1 - 2 \cdot J23 + J4)\end{aligned} \tag{24}$$

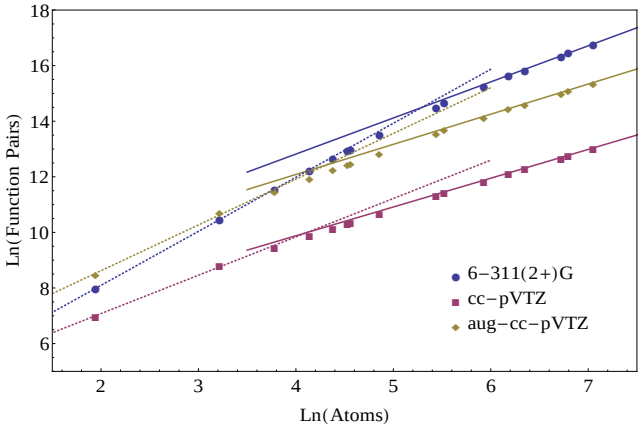

Figure 1: Scaling of the significant basis function pairs with system size (He_7 to He_{1159}). A linear fit to the last five points on each curve gives slopes of 1.3, 1.0 and 1.1 for the custom 6-311(2+)G (11 functions/atom), standard aug-cc-pVTZ (23 functions/atom) and cc-pVTZ (14 functions/atom) basis sets respectively. The dashed lines are fits to the first 3 points to illustrate the onset of basis function sparsity

.

Due to the fragment-blocking of the ALMO MO coefficient matrix, the necessary AO-ERI's to evaluate the unprojected contribution, $(\psi_i\underline{\psi_a}\,|\,\psi_j\underline{\psi_b})$ (i.e. $J1$), will be just the $(\chi_\mu\underline{\chi_\nu}\,|\,\chi_\lambda\underline{\chi_\sigma})$ subset.

Similarly, the exchange term, $(\,\overbrace{\psi_i\psi_j\,|\phi_a\phi_b}\,)$, of Eq. (17) can be written as:

$$\begin{aligned}(\,\overbrace{\psi_i\psi_j\,|\phi_a\phi_b}\,) =& \mathcal{N}_a\mathcal{N}_b\Big\{(\,\overbrace{\psi_i\psi_j\,|\psi_a\psi_b}\,) \\ & -2\,(\,\overbrace{\psi_i\psi_j\,|\psi_a\psi_k}\,)\,(\psi^k\,|\psi_b) + (\psi_i\overbrace{\psi_j\,|\,\psi_k\psi_l}\,)\,(\psi^k\,|\psi_a)\,(\psi^l\,|\psi_b)\Big\} \\ K =& N^2(K1 - 2\cdot K23 + K4) \end{aligned} \tag{25}$$

Here the $(\,\overbrace{\chi_\mu\chi_\nu\,|\chi_\lambda\chi_\sigma}\,)$ AO-ERI's are all that are needed for the unprojected ALMO contributions ($(\,\overbrace{\psi_i\psi_a\,|\psi_j\psi_b}\,)$ or $K1$). This is true even if all $\mathcal{O}(M^4)$ AO-ERI's are non-zero.

These results suggest that we should evaluate the *unprojected* contributions to the ALMO-CIS Coulomb and exchange integrals by fragment-blocked transformation of the $\mathcal{O}(M^2)$ required AO-ERI's, and then correct separately. The unprojected ALMO-CIS integrals will

therefore require only $\mathcal{O}(M^2)$ computational effort. The corrections for projection require evaluating ALMO integrals with 3 occupied indexes, $(\,\underline{\psi_i\psi_a}\,|\psi_j\psi_k)$, $(\,\underline{\psi_i\psi_j}\,|\underline{\psi_a}\psi_k)$, and 4 occupied indexes, $(\psi_i\psi_k\,|\,\psi_j\psi_l)$. These corrections are significantly smaller in magnitude and can be evaluated using the resolution of the identity (RI) approximation without significant loss of accuracy.[76,77] Doing these corrections via RI avoids the need for larger numbers of 4-center AO-ERI's and permits the efficiency of dense linear algebra.

3.3 ALMO Integral Evaluation

The half-transformed integrals $J^{ia}_{\underline{\mu\nu}} = (\underline{\psi_i\psi_a}\,|\,\underline{\chi_\mu\chi_\nu})$ and $K^{ia}_{\underline{\mu\nu}} = (\,\overbrace{\psi_i\underline{\chi_\mu}\,|\underline{\psi_a}\chi_\nu}\,)$ are computed within Q-Chem's AO-ERI evaluation code, which uses the PRISM algorithm for efficiency.[78–80] We have added a customized ERI "digestor" that carries out first two MO quarter-transformations on a batch of AO-ERI's. The batch size is determined by the integral code and does not scale with the size of the system. The fully-transformed integrals are then formed from the half-transformed integrals externally.

Only the integrals with ψ_i and ψ_a on F_I, and χ_μ and χ_ν on F_J are required (corresponding to $(\underline{\chi_\mu\chi_\nu}\,|\,\underline{\chi_\lambda\chi_\sigma})$ and $(\,\overbrace{\chi_\mu\underline{\chi_\nu}\,|\underline{\chi_\lambda}\chi_\sigma}\,)$ as discussed in the previous subsection). No additional truncation is possible within the coulomb integrals, but for the exchange contributions, using the Schwarz integrals, only AO-ERI's with significant overlap need be computed. By creating mini-lists of the required half-transformed integrals we avoid forming many of the AO integrals.[24,81]

The AO integrals are efficiently transformed using customized digestor algorithms. The coulomb digestor, is outlined in algorithm 1 and the exchange digestor, is shown in algorithm 2. These algorithms are shown schematically rather than exactly as implemented in order to avoid undue complexity. In particular, the production code is organized into loops over different angular momentum classes for bras and kets, and then loops over the different shell quartets corresponding to the current bra and ket angular momentum. Finally batches

of selected shell quartets are evaluated. By contrast, the simplified schematics shown in algorithm 1 and algorithm 2 show only loops over AO function pairs.

Algorithm 1: Coulomb digestor for integrals, $J_{\underline{ia}\underline{\lambda\sigma}} = \left(\underline{\psi_i \psi_a} \mid \underline{\chi_\lambda \chi_\sigma}\right)$

for $\underline{\mu\nu} \in F_I$ **do**
  for $\underline{\lambda\sigma}$ *batches* **do**
    Make $\left(\underline{\mu\nu} \mid \underline{\lambda\sigma}\right)$ for $\underline{\mu\nu}$, $\underline{\lambda\sigma}$
    for $\underline{\lambda\sigma} \in$ *batch* **do**
      $F_J \leftarrow \underline{\lambda\sigma}$
      $J_{\underline{ia}\underline{\lambda\sigma}} \mathrel{+}= \left(\underline{\mu\nu} \mid \underline{\lambda\sigma}\right) P^{\overline{\mu\nu}}_{\underline{ia}}, \;\; \forall\, \overline{ia} \in F_I$
      $J_{\underline{jb}\underline{\mu\nu}} \mathrel{+}= \left(\underline{\mu\nu} \mid \underline{\lambda\sigma}\right) P^{\overline{\lambda\sigma}}_{\underline{jb}}, \;\; \forall\, \overline{jb} \in F_J$

For the coulomb integrals a batch of AO integrals are contracted with the transition densities $P^{\overline{\mu\nu}}_{\underline{ia}} = c^{\mu}_{i} c^{\nu\dagger}_{a}$. Each integral batch corresponds to a single bra, $\langle \chi_\mu \chi_\nu |$, so each of its members can be identified with a specific ket, $|\chi_\lambda \chi_\sigma\rangle$. Here λ and σ must belong to the same fragment F_J. Thus, the loop over excitations $\underline{jb}$ only includes those on F_J. The digestor loops over the elements of the batch and identifies the corresponding fragment F_J. This is followed by gathering the relevant elements of the density matrix for the ket side belonging to F_J, $P^{\overline{\lambda\sigma}}_{\underline{jb}}$. Note that the density matrix is symmetrized and vectorized by fragment to further increase the efficiency. Then matrix multiplication between the AO integrals and the density matrix is performed, also accounting for the symmetry of the integrals and the half-transformed integrals $J_{\underline{\mu\nu}\underline{jb}}$ are incremented.

The digestor for the coulomb-like terms uses a symmetrized transition density and yields a half-transformed matrix that is also symmetrized. By contrast, the exchange terms (algorithm 2) cannot accept a symmetrized density, and result in an unsymmetric half-transformed tensor. Thus all symmetries must be accounted for explicitly. It is also important to em-

Algorithm 2: Exchange integrals, $K_{\underset{\frown}{ia}\underset{\frown}{\nu\lambda}} = (\ \overbrace{\psi_i \chi_\nu\,|\psi_a \chi_\lambda}\ )$

for $\mu\nu$ **do**

  for $\lambda\sigma$ *exchange batches* **do**

    $F_I \leftarrow \lambda$, $F_J \leftarrow \sigma$

    Make $(\ \overbrace{\mu\nu\,|\lambda\sigma}\ )$ for $\mu\lambda \in F_I$, $\nu\sigma \in F_J$

    for $\lambda\sigma \in$ *batch* **do**

      $K_{\underset{\frown}{jb}\underset{\frown}{\mu\lambda}} \mathrel{+}= (\ \overbrace{\mu\nu\,|\lambda\sigma}\ )\, P^{\overset{\frown}{\nu\sigma}}_{\underset{\frown}{jb}}, \quad \forall\, \overset{\frown}{jb} \in F_J$

      $K_{\underset{\frown}{jb}\underset{\frown}{\lambda\mu}} \mathrel{+}= (\ \overbrace{\mu\nu\,|\lambda\sigma}\ )\, P^{\overset{\frown}{\sigma\nu}}_{\underset{\frown}{jb}}, \quad \forall\, \overset{\frown}{jb} \in F_J$

      $K_{\underset{\frown}{ia}\underset{\frown}{\nu\sigma}} \mathrel{+}= (\ \overbrace{\mu\nu\,|\lambda\sigma}\ )\, P^{\overset{\frown}{\mu\lambda}}_{\underset{\frown}{ia}}, \quad \forall\, \overset{\frown}{ia} \in F_I$

      $K_{\underset{\frown}{ia}\underset{\frown}{\sigma\nu}} \mathrel{+}= (\ \overbrace{\mu\nu\,|\lambda\sigma}\ )\, P^{\overset{\frown}{\lambda\mu}}_{\underset{\frown}{ia}}, \quad \forall\, \overset{\frown}{ia} \in F_I$

    if $F_I == F_J$ **then**

      for $\lambda\sigma \in$ *batch*, $\overset{\frown}{ia} \in F_I$ **do**

        $K_{\underset{\frown}{ia}\underset{\frown}{\mu\sigma}} \mathrel{+}= (\ \overbrace{\mu\nu\,|\lambda\sigma}\ )\, P^{\overset{\frown}{\nu\lambda}}_{\underset{\frown}{ia}}$

        $K_{\underset{\frown}{ia}\underset{\frown}{\sigma\mu}} \mathrel{+}= (\ \overbrace{\mu\nu\,|\lambda\sigma}\ )\, P^{\overset{\frown}{\lambda\nu}}_{\underset{\frown}{ia}}$

        $K_{\underset{\frown}{ia}\underset{\frown}{\nu\lambda}} \mathrel{+}= (\ \overbrace{\mu\nu\,|\lambda\sigma}\ )\, P^{\overset{\frown}{\mu\sigma}}_{\underset{\frown}{ia}}$

        $K_{\underset{\frown}{ia}\underset{\frown}{\lambda\nu}} \mathrel{+}= (\ \overbrace{\mu\nu\,|\lambda\sigma}\ )\, P^{\overset{\frown}{\sigma\mu}}_{\underset{\frown}{ia}}$

phasize in addition to computational costs which only grow as $\mathcal{O}(M^2)$ even when there are as many as $\mathcal{O}(M^4)$ significant AO-ERI's, these routines are also designed to ensure at most $\mathcal{O}(M^2)$ storage requirements. Both the input transition densities and the output half-transformed matrices are stored in packed format keeping only the required values. Finally, while not shown explicitly, the final two quarter transformations are also done making use of the ALMO locality and scale no higher than $\mathcal{O}(M^2)$.

3.4 ALMO integral corrections

The smaller terms, which are still critical for accurate evaluation of the two electron integrals from Eqs. (24) and (25) include $J23$, $J4$, $K23$ and $K4$. These will be evaluated using the RI approximation, following algorithms which we describe below.

For compactness, the 3-center density-fit integrals will be denoted as $v_{ijP} = (\psi_i\psi_j \,|\, \chi_P)$ and $v_{iaP} = (\psi_i\psi_a \,|\, \chi_P)$. Similarly, the 2-center ERI's in the auxiliary basis will be denoted as $v_{PQ} = (\chi_P \,|\, \chi_Q)$, while elements of its inverse will be written as v^{PQ}. In this notation, the RI correction terms, first introduced in Eqs. (24) and (25) can be explicitly written as follows:

$$J23 = v_{iaP} v^{PQ} v_{jkQ} \sigma_b^k \tag{26}$$

$$J4 = \sigma_a^k v_{ikP} v^{PQ} v_{jlQ} \sigma_b^l \tag{27}$$

$$K23 = v_{ijP} v^{PQ} v_{akQ} \sigma_b^k \tag{28}$$

$$K4 = v_{ijP} v^{PQ} v_{klQ} \sigma_a^k \sigma_b^l \tag{29}$$

There are two primary steps to determine these correction terms. First the RI integrals must be generated and then they are combined to form the final corrections. The RI integrals in the AO basis are formed in batches and subsequently transformed using a customized digestor within the AOints module of Q-Chem, shown in algorithm 3. Two types of inte-

grals are needed, those with both indices occupied, v_{ijP}, and those with one occupied and one virtual, v_{iaP}. The number of occupied-occupied integrals that are required will grow linearly with respect to system size in large enough systems, since ψ_i and ψ_j are both highly localized on their respective fragments and therefore do not have a large spatial extent. The number of pairs of occupied-virtual integrals will be much larger as the virtual orbitals are significantly more diffuse, however, they are still ALMOs and retain the associated advantages in efficiency. Using our efficient implementation, the cost to form the transformed 3-center ERI's does not exceed $\mathcal{O}(M^3)$ with system size. By computing, only the significant occupied-occupied RI integrals the final combination of the integrals to form the correction terms can also be made to scale as $\mathcal{O}(M^3)$ with system size or lower.

In generating the 3-center AO integrals, the auxiliary basis consisting of N_{aux} functions is partitioned into N_{bat} batches based on shell structure to avoid memory issues. Due to this batching policy, the three-center integrals are formed in the "shell" order (i.e. sorted by angular momentum) of the auxiliary basis. Conventionally when writing to disk the digested (ALMO-transformed) integrals are transformed back into their "natural order" (i.e. sorted by atoms). With this approach, considering the $(\psi_i\psi_a \,|\, \chi_P)$ case, only V elements can be continuously written at a time, and thus file writing will be performed $O \times N_{aux}$ times in total (O = number of occupied orbitals). The low efficiency of this seek-dominated I/O procedure eventually causes this to be the rate-determining step of the ALMO-CIS calculation for large systems. Simply writing the full batch of digested integrals (with fixed index i) to disk without reordering enables more data ($V \times N_{aux}$) to be transferred to disk at once and significantly reduces (by N_{aux}/N_{bat}) the time spent in file writing, due to greatly reduced numbers of seeks. The improved I/O efficiency ensures that the expected computational scaling may be obtained. The two-center integrals v_{PQ} should be formed in the same order to ensure consistency of auxiliary basis ordering, which can be realized by a few simple modifications of the existing code without additional cost.

Algorithm 3: 3-center integrals v_{ijP}, v_{iaP}

```
for n = 1, N_bat do
    for μν = 1, (NN) do
        calculate (μν | P)
        F_I ← μ
        for i = 1, o do
            if (i | ν) > thresh then
                for P = 1, N_aux do
                    (iν | P) += (μν | P) · c_i^μ
    for i = 1, O do
        for jν = 1, On do
            if (i | j) > thresh then
                for P = 1, N_aux do
                    (ij | P) += (iν | P) · c_j^ν
        write (ij | P) to disk in order i,P,j (slow to fast) for i, ∀j(significant), P ∈ N_aux
    for i = 1, O do
        for aν = 1, Vn do
            for P = 1, N_aux do
                (ia | P) += (iν | P) · c_a^ν
        write (ia | P) to disk in order i,P,a (slow to fast) for i, ∀a, P ∈ N_aux
```

Algorithm 4: RI Corrections

for $ij = 1, (OO)$ **do**
  for $P = 1, N_{aux}$ **do**
    for $Q = 1, N_{aux}$ **do**
      $c_{ij}^{P} \mathrel{+}= v^{PQ} \cdot v_{ijQ}$

for $ij = 1, (OO)$ **do**
  for $kl = 1, (OO)$ **do**
    for $P = 1, N_{aux}$ **do**
      $\mathscr{V}_{ijkl} \mathrel{+}= c_{ij}^{P} \cdot v_{klP}$

for $ia = 1, Ov$ **do**
  for $jk = 1, (OO)$ **do**
    for $P = 1, N_{aux}$ **do**
      $\mathscr{V}_{iajk} \mathrel{+}= c_{jk}^{P} \cdot v_{iaP}$

for $ia = 1, Ov$ **do**
  for $jk = 1, (OO)$ **do**
    if $(i \mid j) >$ thresh **then**
      for $P = 1, N_{aux}$ **do**
        $\mathscr{V}_{ijak} \mathrel{+}= c_{ij}^{P} \cdot v_{akP}$

The first steps of the RI integral transformation are common to both the coulomb and exchange terms and are shown in algorithm 4. Algorithm 5 then shows the steps for computing the coulomb corrections. For transparency of computational cost, all multiplications are written as loops. Those that grow in cost linearly with the size of the system are in purple, while blue loops are over sparse indices that scale quadratically for small systems but linearly for large systems. The exchange corrections are computed similarly (algorithm 6). These transformations will grow asymptotically as $\mathcal{O}(M^3)$, which is the same scaling as for the matrix diagonalization. However, for small systems they will scale quartically as the full benefits from using ALMOs do not appear immediately.

Algorithm 5: Coulomb RI Corrections

for $ia = 1, Ov$ **do**
  for $jl = 1, (OO)$ **do**
    for $k = 1, O$ **do**
      if $(k \mid i) >$ thresh **then**
        $\mathscr{W}_{\underline{ia}\underline{jl}} \mathrel{+}= \mathscr{V}_{\underline{ikjl}} \cdot \sigma_{\underline{a}}^{\underline{k}}$
  for $jb = 1, Ov$ **do**
    for $l = 1, O$ **do**
      if $(j \mid l) >$ thresh **then**
        $J23_{\underline{ia}\underline{jb}} \mathrel{+}= \mathscr{V}_{\underline{ia}\underline{jl}} \cdot \sigma_{\underline{b}}^{\underline{l}}$
        $J4_{\underline{ia}\underline{jb}} \mathrel{+}= \mathscr{W}_{\underline{ia}\underline{jl}} \cdot \sigma_{\underline{b}}^{\underline{l}}$

4 Results

We employ helium clusters as test systems to explore the accuracy and computational cost of the ALMO-CIS method. With these results in hand, we then use our method to examine the size-dependence of electronic spectrum associated with the $n = 2$ Rydberg levels. As discussed in the introduction, helium clusters appear likely to be suitable for the ALMO-

Algorithm 6: Exchange RI Corrections

```
for ia = 1, Ov do
    for j = 1, O do
        if (i | j) > thresh then
            for kl = 1, (OO) do
                W_ijal += V_ijkl · σ_a^k
    for jb = 1, Ov do
        for l = 1, O do
            K23_ijab += V_ijal · σ_b^l
            K4_ijab  += W_ijal · σ_b^l
```

CIS method because the high ionization potential and negative electron affinity make the discarded charge-transfer (CT) configurations high in energy relative to the retained atomic excitations. Therefore we expect CT effects to be secondary. Tests to explore this question are reported in section 4.1 by comparing ALMO-CIS to standard CIS for medium sized He_{25} clusters. In section 4.2, a detailed analysis of the computational performance of the code is reported, spanning clusters from 7 to 485 atoms. With these characterizations in hand, we turn in section 4.3 to a pilot application of the ALMO-CIS method, on the size-dependence of the excitation spectrum.

4.1 Accuracy

To determine the accuracy of ALMO-CIS it was first applied to small 25-atom clusters which have previously been studied in depth using CIS.[58,59] For the $n = 2$ manifold, 100 states are required to fully characterize the band, with the lowest 25 states having being characterized primarily by superpositions of $2s$-type orbitals and the remaining 75 as $2p$-type. Figure 2 shows a first comparison of the excitation spectrum calculated with full CIS against the simplified ALMO-CIS model, at a single local minimum of He_{25}. It is evident that the general form of the spectrum is entirely preserved by ALMO-CIS: a clear distinction

remains between the 25 states of $2s$ character, and the 75 states of $2p$ character. This is an encouraging validation of the ALMO-CIS model.

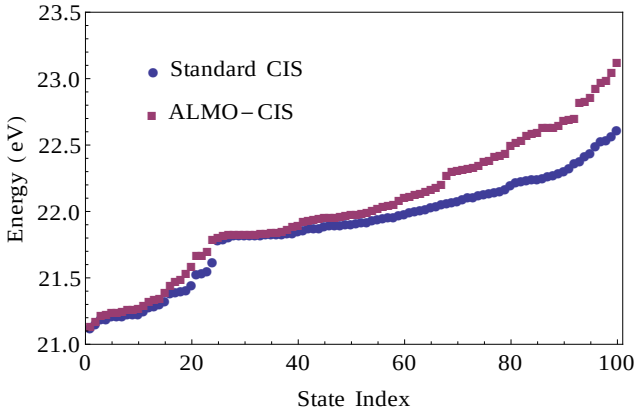

Figure 2: Excitation energy for a single geometry of He_{25} as a function of increasing state, evaluated by CIS and the ALMO-CIS model, for the 100 states in the $n = 2$ Rydberg manifold. A modified 6-311(2+)G basis with 11 functions per He atom was employed.[58] He_{25} states 1-25 are predominantly of $2s$ character and states 26-100 are predominantly of p character. It is evident that ALMO-CIS is nearly identical to CIS for the lowest energy $2s$ and $2p$ states while the maximum error occurs for the states at the blue end of the excited $n = 2$ band.

In slightly more detail, one sees that the low energy part of the $2s$ and $2p$ state manifolds is systematically more accurately reproduced by ALMO-CIS than the high-energy part. The error, of course, is entirely due to charge transfer. It is therefore quite logical that the higher up we are in the manifold, the greater the error will be due to neglect of CT, because those discarded ionic configurations are gradually becoming separated by smaller energy differences from the state of interest. It is also reasonable that errors in the $2p$ manifold are larger than the $2s$ manifold simply because this is a higher energy window, and therefore CT corrections can contribute greater energy stabilization.

These conclusions transfer to other geometries. As can seen in fig. 3 for five sample configurations of the He_{25} cluster, the ALMO-CIS errors, measured against CIS, are qualitatively consistent from geometry to geometry, and begin very small at the red end of both the $s-$ and $p-$manifolds and increase with increasing state number. The maximum error is

0.4-0.5 eV ($< 2.5\%$), which is non-negligible, but less than the standard CIS error of ≈ 1 eV. For application purposes, however, the important point is that the errors all have the same sign, and increase gently and systematically from state to state. This suggests that a qualitatively correct spectrum will be obtained, with highest accuracy at the red edge, and exaggerated width of the blue tail of particularly the $2p$ manifold. The ALMO-CIS spectrum can ultimately be corrected by appropriate scaling.

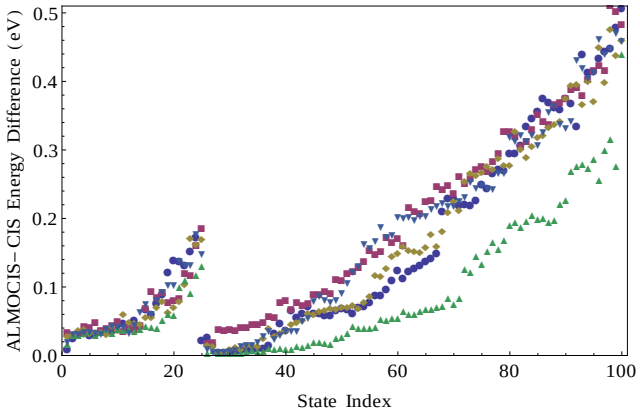

Figure 3: $E_{(ALMO-CIS)} - E_{(CIS)}$: This plot shows the excitation energy differences (eV) between ALMO-CIS and CIS as a function of state for 5 different He_{25} ground state geometries (ie. local minima). He_{25} states 1-25 are s-like and states 26-100 are p-like. ALMO-CIS is nearly identical to CIS for the lowest energy $2s$ and $2p$ states. The maximum errors occurs for the states at the blue end of the excited $2p$ manifold.

The spectrum for He_{25} at the CIS/6-311(2+)G level of theory was previously computed[58] using 100 randomized clusters with geometries optimized using Møller-Plesset perturbation theory (MP2/6-311G). As $1s \rightarrow 2s$ transitions are symmetry forbidden, the s states of the cluster only contribute weakly to the optical spectrum, which is dominated by a broad peak corresponding to the cluster p states. This peak has the atomic excitation energy as its lower bound, and spreads over a range of nearly 2 eV. Using these same structures for the ALMO-CIS/6-311(2+)G spectrum we obtain the results shown in fig. 4, which are compared against the corresponding CIS spectrum.

Qualitatively, the results shown in fig. 4 are exactly as we would have anticipated based

on inspecting the CIS and ALMO-CIS excitation energies for a single configuration in fig. 2, or the ALMO-CIS errors for 5 different configurations shown in fig. 3. In the lowest excited states of the 25-atom clusters (red end of the spectrum), very little error is introduced by the ALMO-CIS approximation. On the other other hand, as discussed previously, the blue tail of the ALMO-CIS spectrum is extended to higher energies relative to the CIS spectrum. Interestingly, there is a second effect also, which is that we see a loss of integrated oscillator strength in the $2p$ band calculated by ALMO-CIS relative to CIS. It may be directly inferred that the neglected CT configurations do contribute non-negligibly to oscillator strength even in the low energy part of the $2p$ band where they contribute very little to the excitation energy. However, the relative intensities throughout the band are generally preserved, which justifies qualitative comparisons.

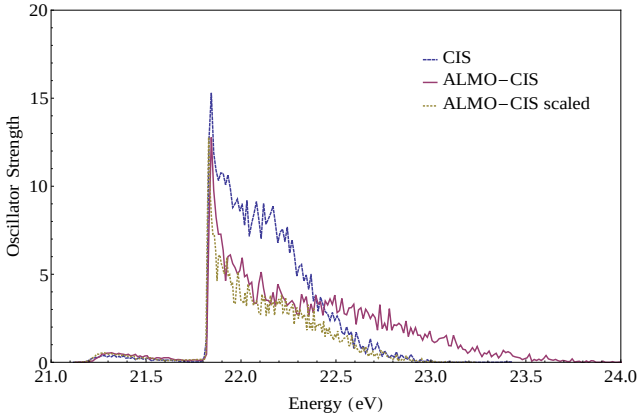

Figure 4: Absorption spectra calculated for a He_{25} cluster at the CIS (solid blue) and ALMO-CIS (solid pink) level of theory. The dashed gold curve shows the ALMO-CIS spectrum where the energies have been corrected by the systematic error

Further physical insight into the origin of the deviations can be obtained from the detailed analysis of the CIS spectrum reported previously.[58] It was determined that the states at the higher energy edge of the spectrum tend to arise from excitations of atoms in the center of the cluster, while the low energy edge (near the atomic excitation energy) correspond to atoms at the surface. The extended $2s$ and $2p$ Rydberg orbitals of a bulk atom overlap the

ground state $1s$ orbital of their neighbors, destabilizing the cluster by Pauli repulsion. It is reasonable to expect states dominated by these bulk contributions to be most affected by charge-transfer, because they better overlap with those from other atoms to yield more significant matrix elements for CT.

4.2 Timings

The main advantage of the ALMO-CIS method is that it theoretically has a very low computational cost: $\mathcal{O}(M^3)$ as a function of cluster size for the full eigenspectrum. This is in contrast with the $\mathcal{O}(M^6)$ computational effort associated with obtaining all eigenstates with standard CIS. As discussed in section 3.1 the diagonalization step is straightforwardly third order in system size. However, significant effort is required to formulate an efficient algorithm for the evaluation of the matrix elements to realize $\mathcal{O}(M^3)$ scaling in practice. The timings reported here result from calculations using a single core on an AMD Opteron 6300 series using helium clusters ranging from He_{44} to He_{485} regularly spaced atoms (4 Å), using the same customized 6-311(2+)G basis as the previous subsections.

Overall the method scales as desired (table 1), revealing overall growth of computational effort just below $\mathcal{O}(M^3)$ in the size range from He_{44} to He_{485}. The results obtained for the relative magnitude of the ALMO-CIS components can be seen in fig. 5. It is evident that while matrix diagonalization is strictly $\mathcal{O}(M^3)$, it has such a low prefactor that it is the least important of the major computational steps in this size regime.

Table 1: Theoretical and actual scaling for total ALMO-CIS calculation and diagonalization

Component	Scaling	
	Predicted	Observed
Diagonalization	M^3	2.88
Total	M^3	2.71

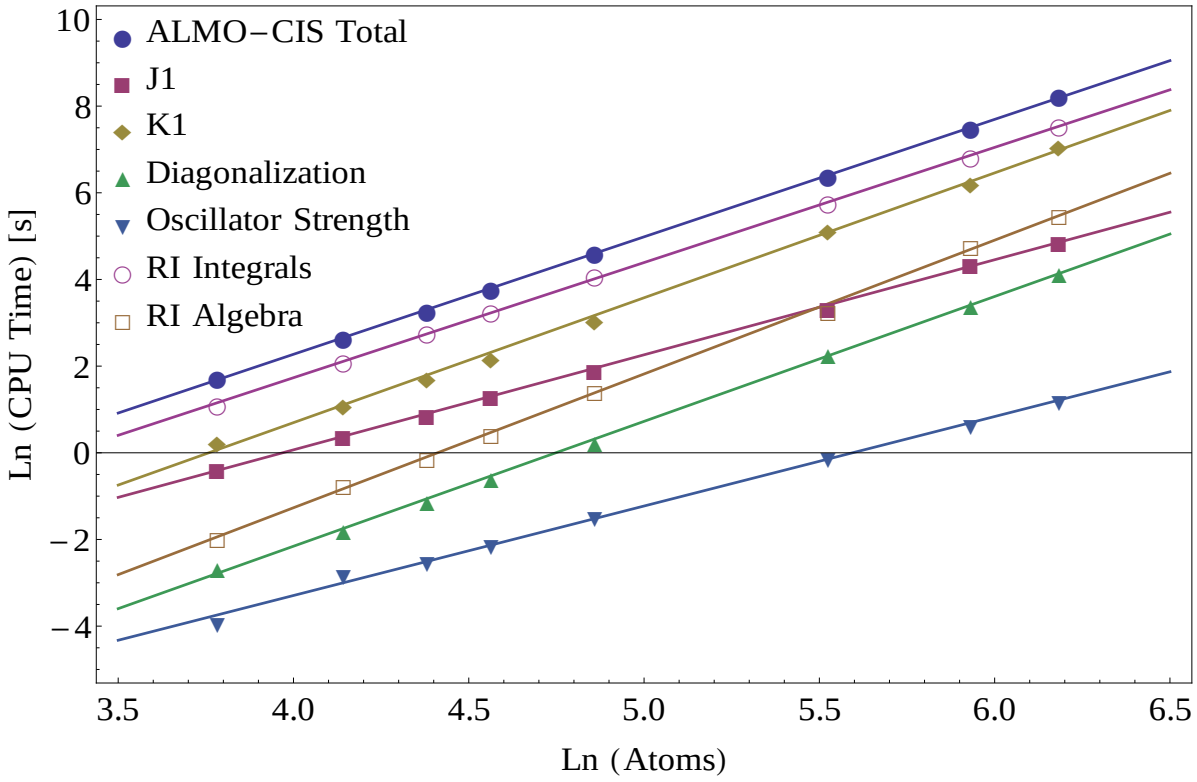

Figure 5: CPU timing data for ALMO-CIS. The clusters in this plot range from 44-485 atoms. The slope of the line corresponding to the total ALMO-CIS time is 2.71, indicating that the scaling is overall $\mathcal{O}(M^3)$ in computational effort, as a function of the number of atoms, M.

Table 2: Theoretical and actual scaling for the formation of J1 and K1. Capital letters scale with the size of the system, lowercase letters are constant and based on the identity of the fragments, N, O, V and M are the number of basis functions, occupied orbitals, virtual orbital and system size respectively. Parentheses indicate sparse matrix scaling: these scale quadratically for small systems and linearly otherwise.

Component	Memory doubles	Scaling Predicted	Scaling Observed
$(\phi_i\psi_a \mid \chi_\mu\chi_\nu)$	$NOnv$	NOn^3	2.16
$(\phi_i\psi_a \mid \phi_j\chi_\nu)$	O^2nv	O^2n^2v	1.99
$(\phi_i\psi_a \mid \phi_j\psi_b)$	O^2v^2	O^2nv^2	1.91
$J1$ Total	M^2	M^2	2.19
$(\overbrace{\phi_i\chi_\mu \mid \psi_a\chi_\nu})$	$(NO)nv$	$(NN)n^2o$	2.89
$(\overbrace{\phi_i\phi_j \mid \psi_a\chi_\nu})$	$(OO)nv$	$(OO)n^2v$	1.96
$(\overbrace{\phi_i\chi_\mu \mid \psi_a\chi_\nu})$	$(OO)v^2$	$(OO)nv^2$	2.00
$K1$ Total	(MM)	(MM)	2.88

The costs of the formation of $J1$ and $K1$ (the unprojected direct and exchange integrals defined in eqs. (24) and (25)) are summarized in table 2. None of these steps should scale worse than $\mathcal{O}(M^2)$ with the system size, as we have designed our implementation to satisfy this criterion. $J1$ is most efficient because selection of significant ERI's can be done immediately at the shell pair level, and, relative to $K1$, only one quarter as many floating point operations are required per significant ERI. On the other hand, $K1$ technically has (NN) sparsity meaning that only a linear number significant matrix elements are required for large enough systems. However, our present shell quartet selection algorithm is based on all *fragment pairs* and does not include screening based on fragment pairs that give vanishing $K1$ contributions, thus it scales as $\mathcal{O}(M^2)$.

The costs associated with forming the RI integrals and subsequently assembling the correction terms are given in table 3. These are unavoidably third order steps, and implemented this way, as observed in the timings. The most costly $\mathcal{O}(M^3)$ steps are the formation of the RI integral terms v_{ijP} and v_{iaP} as is clear from fig. 5. Their cost could still be reduced by approximately a factor of two, by reusing the $(\chi_\mu\chi_\nu \,|\, \chi_P)$ terms, and there may be additional pre-factor reductions that are possible. These optimizations will not affect the overall scaling. Thus, we successfully created an algorithm for computing excited states of clusters, which scales $\mathcal{O}(M^3)$. We have applied this code for timing purposes in calculations on as many as 485 atoms and 5335 basis functions, to obtain 4850 excited states. We believe that excited state calculations of this scale have not hitherto been reported.

4.3 Size-dependence of the excitation spectrum of helium clusters

In the ground state, the superfluidic phase can be distinguished for clusters with greater than or equal to about 60 atoms.[51] Additionally, it is predicted that clusters in the regime of ≈ 500 atoms begin displaying bulk-like properties.[82] Thus, clusters containing $10^2 - 10^3$ atoms are particularly interesting as they span this boundary region where observable properties are

Table 3: Theoretical and actual scaling for RI integrals and formation of correction terms $J23$, $J4$, $K23$, $K4$. Notation as in table 2, with the addition of X for the number of auxiliary functions. Where multiple steps are involved the most costly step is indicated.

Component	Rate limiting step	Memory doubles	Scaling	
			Predicted	Observed
$\left(\chi^Q \mid \chi^P\right)$	matrix inversion	X^2	X^3	2.82
$(\phi_i\phi_j \mid \chi_P)$	$(\chi_\mu\chi_\nu \mid \chi_P)$	$(OO)X^*$	$(NN)X$	2.55
$(\phi_i\psi_a \mid \chi_P)$	$(\chi_\mu\chi_\nu \mid \chi_P)$	OVX^*	$(NN)X$	2.66
c_{kl}^P	$v^{PQ}v_{klQ}$	$(OO)X$	$(OO)X^2$	3.06
$\mathscr{V}_{ijkl}$	$c_{ij}^P v_{klP}$	$(OO)^2$	$(OO)^2X$	3.25
$\mathscr{V}_{ia\underline{\ }jk}$	$v_{ia\underline{\ }P}c_{jk}^P$	$Ov(OO)$	$Ov(OO)X$	3.10
$\mathscr{V}_{ij\underline{\ }ak}$	$c_{ij}^P v_{a\underline{\ }kP}$	OvO^2	$Ov(OO)X$	3.14
$J23$	$\mathscr{V}_{ia\underline{jk}} \cdot \sigma_{\underline{b}}^k$	O^2v^2	$Ov(OO)v$	1.88
$J4$	$\sigma_{\underline{a}}^k \cdot \mathscr{V}_{ik\underline{jl}} \cdot \sigma_{\underline{b}}^l$	O^2v^2	$(OO)^2v$	2.29
$K23$	$\mathscr{V}_{\underline{ij}\underline{\ }\underline{ak}} \cdot \sigma_{\underline{b}}^k$	O^2v^2	$(OO)Ov^2$	2.06
$K4$	$\sigma_{\underline{a}}^k \cdot \mathscr{V}_{\underline{ij}kl} \cdot \sigma_{\underline{b}}^l$	O^2v^2	$(OO)^2v$	2.94

* In practice, the full set of 3-center integrals never exist in memory at one time, because they are computed in batches. The numbers demonstrated here are actually the space required for disk saving.

likely to be changing. Previous theoretical studies of excited states of helium were only able to utilize clusters with ≤ 25 atoms due to the computational cost of calculating the large number of excited states required.[58,59,83]

The size-dependence of the helium cluster excitation spectrum is an ideal pilot application for ALMO-CIS. Earlier work on the spectra of He_7 and He_{25} clusters produced results that compared very favorably with previous experiments, when the geometries of the ground state clusters are optimized with MP2/6-311G.[58] In larger clusters nuclear quantum effects become increasingly important and not accounting for them results in over-structured clusters. Here we consider clusters an order of magnitude larger (e.g. He_{231}) where MP2 optimizations are impractical, thus, as the ground state structures are not critical to demonstrate the utility of ALMO-CIS, the cluster sampling was done with classical dynamics. For this paper, all geometries were obtained using the Optimize program in Tinker[84] after randomly perturbing an initial structure with atoms regularly spaced 4 Å apart. A He-He Lennard-Jones potential with $r_0 = 3.6$ Å and $\epsilon_0 = 0.05$ K was used for cluster optimization, with parameters adjusted to give reasonable spacing (bulk interatomic spacing in helium clusters is 3.6 Å). Since a tight optimization without zero point energy will give a highly ordered cluster (due to neglect of zero point motion), we used a loose convergence criterion to obtain randomized structures with spacing similar to the known He-He separations in solids and clusters. This should be sufficient for the qualitative study of size-dependent effects; further studies on the states of very large helium clusters are in progress, which account for nuclear effects.

The calculated spectra are shown in fig. 6. It is immediately evident that there are indeed strong size-dependent effects on the absorption spectra. The first effect is an increase in oscillator strength contained in the band, which is simply a reflection of the number of states in the manifold and increases linearly with size of the cluster. The second effect, also related to the oscillator strength, is the emergence of intensity borrowing in the $2s$ manifold

as the cluster size increases. This reflects increased mixing with $2p$ states.

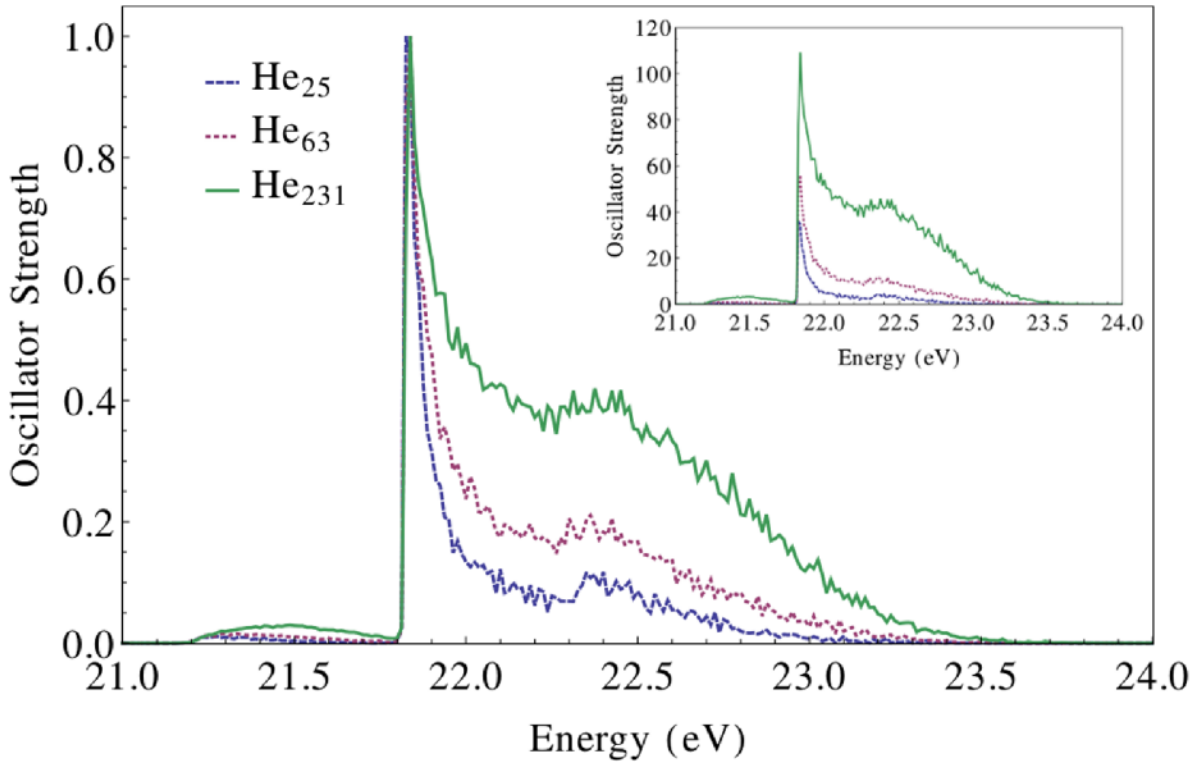

Figure 6: Calculated absorption spectra for He_{231}(solid green), He_{63} (dotted purple) and He_{25} (dashed blue) at the ALMO-CIS level of theory as a function of excitation energy (eV). In the main figure, the spectra are scaled so that the maximum peak height for each size cluster is 1, while the inset shows the unscaled spectrum.

The most interesting size-dependent effects on the absorption spectrum are in the $2p$ band where the width of the manifold increases noticeably with cluster size. Additionally, the median of the oscillator strength shifts from the red edge of the manifold in the small He_{25} cluster towards the middle of the manifold by He_{231}. This unambiguously confirms the assignment of primarily "bulk" character to the states that lie towards the blue end of the manifold, versus those of "surface" character that lie towards the red end of the manifold. The effects of increasing the size of the cluster are primarily due to the increasing importance of the bulk-like states. In the 62- and 231-atom clusters, which contain the highest percentage of bulk states, a hump can be seen clearly forming near 22.4 eV that can be attributed to

states on the interior of the cluster.

We recall from section 4.1, that the main ALMO-CIS error is the exaggerated bandwidth of the manifold, with states on the blue edge increasingly overestimated. It is also possible that this effect increases with the size of the cluster, but since standard CIS cannot be reasonably run on the large clusters with enough states to explore the blue edge, we must leave this issue as an open question. The other result from our tests of ALMO-CIS vs CIS reported in section 4.1 was that neglect of the short-range charge transfer terms certainly leads to an overall underestimate of oscillator strength, which likely becomes more important towards the blue edge as CT contributions become less negligible (though most likely still small).

5 Conclusions

In computations on homogenous atomic and molecular clusters, large numbers of excited states are required to describe the broadening of atomic or molecular excitations into the bands associated with cluster, which gradually evolve towards the bulk limit. This need for many states makes conventional excited state methods particularly costly for such applications. To address this problem, we have developed a physically motivated local variant of configuration interaction with single substitutions (CIS), which retains only intra-fragment single excitations. All inter-fragment singles are discarded. We use the absolutely localized molecular orbitals (ALMO's) to describe occupied and virtual levels of the cluster, and thus term our fragment-localized method as ALMO-CIS. ALMO-CIS is physically appropriate for homogeneous clusters composed of atoms or molecules with high ionization potentials and low or negative electron affinities, as this combination minimizes the importance of the neglected charge-transfer terms.

The main conclusions of our work developing, implementing, testing and applying the

ALMO-CIS model are as follows.

1. **Formal scaling.** Complete construction and diagonalization of the ALMO-CIS Hamiltonian for all eigenvalues and eigenstates scales no worse than $\mathcal{O}(M^3)$ with the number of atoms or molecules, M, in the cluster. By contrast, conventional CIS for all states scales as $\mathcal{O}(M^6)$.

2. **Accuracy for helium cluster absorption spectra.** Testing against full CIS for He_{25} absorption spectra shows good qualitative agreement for the full spectrum, and excellent quantitative agreement at the red edge of the $2s$ and $2p$ manifolds. ALMO-CIS systematically overestimates the excitation energies, with the error gradually increasing to its largest values at the blue edge of the $2p$ manifold, which can be corrected for when needed. When comparing ALMO-CIS to standard CIS there is a clear decrease in total oscillator strength, however, the relative strength across the band is reasonably conserved, and the trend with increasing the cluster size is consistent.

3. **Numerical performance.** We have successfully formulated and implemented an algorithm that is operationally $\mathcal{O}(M^3)$ up to the largest cluster tested (485 atoms), and permits these calculations with 4850 excited states and 5335 basis functions on workstation class computers.

4. **Application to helium cluster absorption spectra.** As a pilot application we evaluated the size-dependence of absorption spectra of helium clusters, and observed a variety of interesting effects that are qualitatively similar to trends seen experimentally. These include an increase in the intensity of the region corresponding to bulk-like states relative to the surface states, and a broadening of the peak.

5. **Further possibilities.** The ALMO-CIS model could benefit from a variety of improvements. Most important is some type of diagnostic or correction for the role of

the neglected charge transfer configurations. Such differences also potentially yield physical insight into the role of CT in excited states. Dynamic correlation is missing, and might be reincorporated either by extending the model to time-dependent density functional theory, or incorporating wave-function based correlation.

6 Acknowledgements

This work was supported by the Director, Office of Science, Office of Basic Energy Sciences, Chemical Sciences Division of the U.S. Department of Energy under Contract no. DEAC02-05CH11231.

References

(1) Serrano-Andrés, L.; Merchán, M. *J. Mol. Struct. THEOCHEM* **2005**, *729*, 99–108.

(2) Dreuw, A. *ChemPhysChem* **2006**, *7*, 2259–2274.

(3) Dreuw, A.; Head-Gordon, M. *Chem. Rev.* **2005**, *105*, 4009–4037.

(4) Casida, M. E.; Huix-Rotllant, M. *Annu. Rev. Phys. Chem.* **2012**, *63*, 287–323.

(5) Cai, Z.-L.; Sendt, K.; Reimers, J. R. *J. Chem. Phys.* **2002**, *117*, 5543–5549.

(6) Grimme, S.; Parac, M. *ChemPhysChem* **2003**, *4*, 292–295.

(7) Dreuw, A.; Head-Gordon, M. *J. Am. Chem. Soc.* **2004**, *126*, 4007–4016.

(8) Niehaus, T. A.; March, N. H. *Theor. Chem. Acc.* **2009**, *125*, 427–432.

(9) Foresman, J. B.; Head-Gordon, M.; Pople, J. A.; Frisch, M. J. *J. Phys. Chem.* **1992**, *96*, 135–149.

(10) Hirata, S.; Head-Gordon, M. *Chem. Phys. Lett.* **1999**, *314*, 291–299.

(11) Head-Gordon, M.; Rico, R.; Oumi, M.; Lee, T. *Chem. Phys. Lett.* **1994**, *219*, 21–29.

(12) Head-Gordon, M.; Oumi, M.; Maurice, D. *Mol. Phys.* **1999**, *96*, 593–602.

(13) Christiansen, O.; Koch, H.; Jø rgensen, P. *Chem. Phys. Lett.* **1995**, *243*, 409–418.

(14) Stanton, J. F.; Gauss, J.; Ishikawa, N.; Head-Gordon, M. *J. Chem. Phys.* **1995**, *103*, 4160–4174.

(15) Krylov, A. I. *Annu. Rev. Phys. Chem.* **2008**, *59*, 433–462.

(16) Rhee, Y.-M.; Head-Gordon, M. *J. Phys. Chem. A* **2007**, *111*, 5314–5326.

(17) Casanova, D.; Rhee, Y. M.; Head-Gordon, M. *J. Chem. Phys.* **2008**, *128*, 164106.

(18) Roos, B. O.; Taylor, P. R.; Siegbahn, P. E. M. *Chem. Phys.* **1980**, *48*, 157–173.

(19) Page, C. S.; Olivucci, M. *J. Comput. Chem.* **2003**, *24*, 298–309.

(20) Casanova, D.; Head-Gordon, M. *Phys. Chem. Chem. Phys.* **2009**, *11*, 9779–9790.

(21) Bell, F.; Zimmerman, P. M.; Casanova, D.; Goldey, M.; Head-Gordon, M. *Phys. Chem. Chem. Phys.* **2013**, *15*, 358–366.

(22) Mayhall, N. J.; Head-Gordon, M. *J. Chem. Phys.* **2014**, *141*, 044112.

(23) Kohn, W. *Phys. Rev. Lett.* **1996**, *76*, 3168–3171.

(24) White, C. A.; Johnson, B. G.; Gill, P. M. W.; Head-Gordon, M. *Chem. Phys. Lett.* **1996**, *253*, 268–278.

(25) Ochsenfeld, C.; White, C. A.; Head-Gordon, M. *J. Chem. Phys.* **1998**, *109*, 1663–1669.

(26) Scuseria, G. E. *J. Phys. Chem. A* **1999**, *103*, 4782–4790.

(27) Goedecker, S. *Rev. Mod. Phys.* **1999**, *71*, 1085–1123.

(28) Baer, R.; Head-Gordon, M. *Phys. Rev. Lett.* **1997**, *79*, 3962–3965.

(29) Yam, C. Y.; Zhang, Q.; Wang, F.; Chen, G. H. *Chem. Soc. Rev.* **2012**, *41*, 3821–3838.

(30) Kjaergaard, T.; Jorgensen, P.; Olsen, J.; Coriani, S.; Helgaker, T. *J. Chem. Phys.* **2008**, *129*, 054106.

(31) Tretiak, S.; Isborn, C. M.; Niklasson, A. M. N.; Challacombe, M. *J. Chem. Phys.* **2009**, *130*, 054111.

(32) Li, Q. X.; Li, Q. K.; Shuai, Z. G. *Synth. Met.* **2008**, *158*, 330–335.

(33) Miura, M.; Aoki, Y. *J. Comput. Chem.* **2009**, *30*, 2213–2230.

(34) Miura, M.; Aoki, Y. *Mol. Phys.* **2010**, *108*, 205–210.

(35) Wu, F. Q.; Liu, W. J.; Zhang, Y.; Li, Z. D. *J. Chem. Theor. Comput.* **2011**, *7*, 3643–3660.

(36) Tsuchiya, T.; Shrestha, K.; Jakubikova, E. *J. Chem. Theory Comput.* **2013**, *9*, 3350–3363.

(37) Svensson, M.; Humbel, S.; Froese, R. D. J.; Matsubara, T.; Sieber, S.; Morokuma, K. *J. Phys. Chem.* **1996**, *100*, 19357–19363.

(38) Senn, H. M.; Thiel, W. *Angew. Chemie-International Ed.* **2009**, *48*, 1198–1229.

(39) Li, X.; Chung, L. W.; Morokuma, K. In *Comput. Methods Large Syst. Electron. Struct. Approaches Biotechnol. Nanotechnol.*; Reimers, J. R., Ed.; John Wiley & Sons, Inc.: Hoboken, New Jersey, 2011; Chapter 12, pp 397–433.

(40) Mata, R. A.; Stoll, H. *J. Chem. Phys.* **2011**, *134*, 034122.

(41) Fedorov, D. G.; Nagata, T.; Kitaura, K. *Phys. Chem. Chem. Phys.* **2012**, *14*, 7562–7577.

(42) Ikegami, T.; Ishida, T.; Fedorov, D. G.; Kitaura, K.; Inadomi, Y.; Umeda, H.; Yokokawa, M.; Sekiguchi, S. *J. Comput. Chem.* **2009**, *31*, 447–454.

(43) Grimme, S. *J. Chem. Phys.* **2013**, *138*, 244104.

(44) Risthaus, T.; Hansen, A.; Grimme, S. *Phys. Chem. Chem. Phys.* **2014**, *16*, 14408–14419.

(45) Liu, J.; Herbert, J. M. *J. Chem. Phys.* **2015**, *143*, 034106.

(46) Helmich, B.; Hättig, C. *J. Chem. Phys.* **2011**, *135*, 214106.

(47) Helmich, B.; Hättig, C. *J. Chem. Phys.* **2013**, *139*, 084114.

(48) Jortner, J. *Z. Phys. D* **1992**, *24*, 247–275.

(49) Castleman Jr., A. W.; Bowen Jr., K. H. *J. Phys. Chem.* **1996**, *100*, 12911–12944.

(50) Bartell, L. S. *Annu. Rev. Phys. Chem.* **1998**, *49*, 43–72.

(51) Grebenev, S.; Toennies, J. P.; Vilesov, A. F. *Science* **1998**, *279*, 2083–2086.

(52) Stienkemeier, F.; Vilesov, A. F. *J. Chem. Phys.* **2001**, *115*, 10119.

(53) Toennies, J. P.; Vilesov, A. F. *Angew. Chem.-Int. Ed.* **2004**, *43*, 2622–2648.

(54) Choi, M. Y.; Douberly, G. E.; Falconer, T. M.; Lewis, W. K.; Lindsay, C. M.; Merritt, J. M.; Stiles, P. L.; Miller, R. E. *Int. Rev. Phys. Chem.* **2006**, *25*, 15–75.

(55) Wang, C. C.; Kornilov, O.; Gessner, O.; Kim, J. H.; Peterka, D. S.; Neumark, D. M. *J. Phys. Chem. A* **2008**, *112*, 9356–9365.

(56) Joppien, M.; Karnbach, R.; Möller, T. *Phys. Rev. Lett.* **1993**, *71*, 2654–2657.

(57) Mudrich, M.; Stienkemeier, F. *Int. Rev. Phys. Chem.* **2014**, *33*, 301–339.

(58) Closser, K. D.; Head-Gordon, M. *J. Phys. Chem. A* **2010**, *114*, 8023–8032.

(59) Closser, K. D.; Gessner, O.; Head-Gordon, M. *J. Chem. Phys.* **2014**, *140*, 134306.

(60) Khaliullin, R. Z.; Head-Gordon, M.; Bell, A. T. *J. Chem. Phys.* **2006**, *124*, 204105.

(61) Stoll, H.; Wagenblast, G.; Preuss, H. *Theor. Chim. Acta* **1980**, *57*, 169–178.

(62) Cullen, J. *Int. J. Quantum Chem. Symp.* **1991**, *25*, 193–207.

(63) Gianinetti, E.; Raimondi, M.; Tornaghi, E. *Int. J. Quantum Chem.* **1996**, *60*, 157–166.

(64) Nagata, T.; Takahashi, O.; Saito, K.; Iwata, S. *J. Chem. Phys.* **2001**, *115*, 3553–3560.

(65) Mo, Y. R.; Gao, J. L.; Peyerimhoff, S. D. *J. Chem. Phys.* **2000**, *112*, 5530–5538.

(66) Khaliullin, R. Z.; Cobar, E. A.; Lochan, R. C.; Bell, A. T.; Head-Gordon, M. *J. Phys. Chem. A* **2007**, *111*, 8753–8765.

(67) Khaliullin, R. Z.; Bell, A. T.; Head-Gordon, M. *J. Chem. Phys.* **2008**, *128*, 184112.

(68) Horn, P. R.; Sundstrom, E. J.; Baker, T. A.; Head-Gordon, M. *J. Chem. Phys.* **2013**, *138*, 134119.

(69) Head-Gordon, M.; Maslen, P. E.; White, C. A. *J. Chem. Phys.* **1998**, *108*, 616–625.

(70) Head-Gordon, M.; Lee, M. S.; Maslen, P. E.; Van Voorhis, T. A.; Gwaltney, S. R. In *Mod. Methods Algorithms Quantum Chem.*; Grotendorst, J., Ed.; John von Neumann Institute for Computing, 2000; Vol. 3; pp 1–46.

(71) Shao, Y.; Molnar, L. F.; Jung, Y.; Kussmann, J.; Ochsenfeld, C.; Brown, S. T.; Gilbert, A. T. B.; Slipchenko, L. V.; Levchenko, S. V.; O'Neill, D. P.; DiStasio, R. a.; Lochan, R. C.; Wang, T.; Beran, G. J. O.; Besley, N. a.; Herbert, J. M.; Lin, C. Y.; Van Voorhis, T.; Chien, S. H.; Sodt, A.; Steele, R. P.; Rassolov, V. a.; Maslen, P. E.; Korambath, P. P.; Adamson, R. D.; Austin, B.; Baker, J.; Byrd, E. F. C.; Dachsel, H.; Doerksen, R. J.; Dreuw, A.; Dunietz, B. D.; Dutoi, A. D.; Furlani, T. R.; Gwaltney, S. R.; Heyden, A.; Hirata, S.; Hsu, C.-P.; Kedziora, G.; Khalliulin, R. Z.; Klunzinger, P.; Lee, A. M.; Lee, M. S.; Liang, W.; Lotan, I.; Nair, N.; Peters, B.; Proynov, E. I.; Pieniazek, P. a.; Rhee, Y. M.; Ritchie, J.; Rosta, E.; Sherrill, C. D.; Simmonett, A. C.; Subotnik, J. E.; Woodcock, H. L.; Zhang, W.; Bell, A. T.; Chakraborty, A. K.; Chipman, D. M.; Keil, F. J.; Warshel, A.; Hehre, W. J.; Schaefer, H. F.; Kong, J.;

Krylov, A. I.; Gill, P. M. W.; Head-Gordon, M. *Phys. Chem. Chem. Phys.* **2006**, *8*, 3172–3191.

(72) Shao, Y.; Gan, Z.; Epifanovsky, E.; Gilbert, A. T.; Wormit, M.; Kussmann, J.; Lange, A. W.; Behn, A.; Deng, J.; Feng, X.; Ghosh, D.; Goldey, M.; Horn, P. R.; Jacobson, L. D.; Kaliman, I.; Khaliullin, R. Z.; Kuś, T.; Landau, A.; Liu, J.; Proynov, E. I.; Rhee, Y. M.; Richard, R. M.; Rohrdanz, M. A.; Steele, R. P.; Sundstrom, E. J.; Woodcock, H. L.; Zimmerman, P. M.; Zuev, D.; Albrecht, B.; Alguire, E.; Austin, B.; Beran, G. J. O.; Bernard, Y. A.; Berquist, E.; Brandhorst, K.; Bravaya, K. B.; Brown, S. T.; Casanova, D.; Chang, C.-M.; Chen, Y.; Chien, S. H.; Closser, K. D.; Crittenden, D. L.; Diedenhofen, M.; DiStasio, R. A.; Do, H.; Dutoi, A. D.; Edgar, R. G.; Fatehi, S.; Fusti-Molnar, L.; Ghysels, A.; Golubeva-Zadorozhnaya, A.; Gomes, J.; Hanson-Heine, M. W.; Harbach, P. H.; Hauser, A. W.; Hohenstein, E. G.; Holden, Z. C.; Jagau, T.-C.; Ji, H.; Kaduk, B.; Khistyaev, K.; Kim, J.; Kim, J.; King, R. A.; Klunzinger, P.; Kosenkov, D.; Kowalczyk, T.; Krauter, C. M.; Lao, K. U.; Laurent, A.; Lawler, K. V.; Levchenko, S. V.; Lin, C. Y.; Liu, F.; Livshits, E.; Lochan, R. C.; Luenser, A.; Manohar, P.; Manzer, S. F.; Mao, S.-P.; Mardirossian, N.; Marenich, A. V.; Maurer, S. A.; Mayhall, N. J.; Neuscamman, E.; Oana, C. M.; Olivares-Amaya, R.; ONeill, D. P.; Parkhill, J. A.; Perrine, T. M.; Peverati, R.; Prociuk, A.; Rehn, D. R.; Rosta, E.; Russ, N. J.; Sharada, S. M.; Sharma, S.; Small, D. W.; Sodt, A.; Stein, T.; Stück, D.; Su, Y.-C.; Thom, A. J.; Tsuchimochi, T.; Vanovschi, V.; Vogt, L.; Vydrov, O.; Wang, T.; Watson, M. A.; Wenzel, J.; White, A.; Williams, C. F.; Yang, J.; Yeganeh, S.; Yost, S. R.; You, Z.-Q.; Zhang, I. Y.; Zhang, X.; Zhao, Y.; Brooks, B. R.; Chan, G. K.; Chipman, D. M.; Cramer, C. J.; Goddard, W. A.; Gordon, M. S.; Hehre, W. J.; Klamt, A.; Schaefer, H. F.; Schmidt, M. W.; Sherrill, C. D.; Truhlar, D. G.; Warshel, A.; Xu, X.; Aspuru-Guzik, A.; Baer, R.; Bell, A. T.; Besley, N. A.; Chai, J.-D.; Dreuw, A.; Dunietz, B. D.; Furlani, T. R.; Gwaltney, S. R.; Hsu, C.-P.;

Jung, Y.; Kong, J.; Lambrecht, D. S.; Liang, W.; Ochsenfeld, C.; Rassolov, V. A.; Slipchenko, L. V.; Subotnik, J. E.; Van Voorhis, T.; Herbert, J. M.; Krylov, A. I.; Gill, P. M.; Head-Gordon, M. *Molecular Physics* **2015**, *113*, 184–215.

(73) Davidson, E. R. *J. Comput. Phys.* **1975**, *17*, 87–94.

(74) Häser, M.; Ahlrichs, R. *J. Comput. Chem.* **1989**, *10*, 104–111.

(75) Kussmann, J.; Ochsenfeld, C. *J. Chem. Phys.* **2013**, *138*, 134114.

(76) Weigend, F.; Häser, M.; Patzelt, H.; Ahlrichs, R. *Chem. Phys. Lett.* **1998**, *249*, 143–152.

(77) Reine, S.; Tellgren, E.; Krapp, A.; Kjaergaard, T.; Helgaker, T.; Jansik, B.; Host, S.; Salek, P. *J. Chem. Phys.* **2008**, *129*, 104101.

(78) Gill, P. M. W.; Pople, J. A. *Int. J. Quantum Chem.* **1991**, *40*, 753–772.

(79) Gill, P. M. W. *Adv. quantum Chem.* **1994**, *25*, 141–205.

(80) Gill, P. M. W.; Gilbert, A. T. B.; Adams, T. R. *J. Comput. Chem.* **2000**, *21*, 1505–1510.

(81) Ochsenfeld, C.; White, C. A.; Head-Gordon, M. *J. Chem. Phys.* **1998**, *109*, 1663–1669.

(82) von Haeften, K.; Laarmann, T.; Wabnitz, H.; Möller, T.; Fink, K. *J. Phys. Chem. A* **2011**, *115*, 7316–7326.

(83) von Haeften, K.; Fink, K. *Eur. Phys. J. D* **2007**, *43*, 121–124.

(84) Ponder, J. W. TINKER *Molecular Modeling Package*, V7.1. 2015.

Supporting Information Available

Full derivation of the matrix elements and resolution of the identity corrections. This material is available free of charge via the Internet at `http://pubs.acs.org/`.

Graphical TOC Entry